THE ASTROPHYSICAL JOURNAL, 410:673–685, 1993 June 20

ANGULAR BROADENING OF PULSARS AND THE DISTRIBUTION OF INTERSTELLAR PLASMA FLUCTUATIONS

C. R. GWINN
Department of Physics, University of California, Santa Barbara, CA 93106; and Harvard-Smithsonian Center for Astrophysics
N. BARTEL
Department of Physics and Astronomy, York University, North York, ON Canada, M3J 1P3 and Harvard-Smithsonian Center for Astrophysics
AND
J. M. CORDES
Department of Astronomy, Cornell University, Space Sciences Building, Ithaca, NY 14853-6801; and Arecibo Observatory, National Astronomy and Ionosphere Center
Received 1992 August 27; accepted 1992 December 17

ABSTRACT

Comparison of angular and temporal broadening for 10 pulsars suggests a uniform distribution of scattering material in the interstellar plasma with localized, strong scattering near young supernova remnants. Angular broadening and temporal broadening both measure the integrated strength of scattering along the line of sight, but with different weighting functions. Comparison of the two thus yields information on the distribution of scattering material along the line of sight.

We report new measurements of angular diameter for the scattering disks of eight pulsars, and discuss two measurements from the literature. We compare these results with published measurements of temporal broadening. Scattering disks of four pulsars are unresolved, but are close to the speckle regime of interstellar scattering. Four of the objects show moderate scattering. In the context of a model consisting of a thin screen superposed on a uniform medium, comparison of angular and temporal broadening suggests that the localized component of scattering has strength ~ 3 times that of the uniform medium.

Signals from the Crab (0531+21) and Vela (0833−45) pulsars are heavily scattered by their surrounding supernova remnants; scattering by the remnants is more than 38 times as strong as by the uniform medium. The fluctuations responsible for this scattering may be associated with cosmic-ray acceleration. We compare strengths and spatial spectra of the scattering material in the supernova remnants that enclose these pulsars, and in the supernova remnant CTB 80, which encloses pulsar 1951+32. Remnants show significant differences in scattering properties.

Subject headings: ISM: structure — pulsars: general — supernova remnants — techniques: interferometric

1. INTRODUCTION

The location of the density fluctuations in the interstellar plasma that are responsible for radio-wave scattering has been a problem of astrophysics since the discovery of scintillation in early observations of pulsars (Scheuer 1968). In this paper we compare temporal broadening and angular broadening of pulsars, due to interstellar scattering, to determine characteristic distances of scattering material. On the basis of this comparison, we argue that some strongly scattering material lies in young supernova remnants; an extended, nearly uniform component is also present. The organization of the paper is as follows. Section 1 discusses previous work on the distribution of scattering material and introduces the basic quantities of scattering. Section 2 outlines the basis of our technique. Section 3 describes our observations and data reduction, and summarizes data taken from the literature. Section 4 compares angular and temporal broadening quantitatively for our data. Section 5 argues that the distribution of scattering material along typical lines of sight 1 to a few kiloparsecs in length is nearly uniform, on the basis of our data; it also shows that strongly scattering material is concentrated near the Crab and Vela supernova remnants and discusses the scattering strength and spatial spectrum of fluctuations in that material. Section 6 summarizes the conclusions of the paper.

1.1. *Distribution of Scattering Material on the Sky*

Observations of the strength of scattering of radio waves by density fluctuations in the interstellar plasma indicate that the scattering material is strongly clumped at low Galactic latitude. The strength of scattering varies smoothly with angle for Galactic latitudes $|b| \gtrsim 10°$, with $1/\sin|b|$ dependence expected for a uniform medium extending to some height above and below the galactic plane (Readhead & Hewish 1972). However, scattering at latitudes $|b| \lesssim 5°$–$10°$ can be much stronger than that expected from extrapolation from higher latitudes and can vary strongly over less than a degree (Dennison et al. 1984; Rao & Ananthakrishnan 1984; Cordes, Weisberg, & Boriakoff 1985). This varying character of the strength of scattering has motivated a two-component model for the scattering material, as discussed quantitatively by Dennison et al., Cordes et al., and Fey, Spangler, & Cordes (1991). Their models include smoothly distributed scattering material extending far above and below the Galactic plane, and additional strongly scattering material, distributed irregularly, near the Galactic plane. These different components presumably correspond to two or more phases of the interstellar medium; Dennison et al. suggest that the more strongly scattering component corresponds to the halos of H II regions (see also Spangler & Gwinn 1990).

The strength of scattering can be quantified in various ways; one common such measure is C_n^2, the coefficient of a Kolmogorov-law spectrum of density fluctuations. For such a spectrum, the spatial power spectrum of electron density fluctuations, $P_{\delta n_e}$, follows a power law over orders of magnitude in spatial wavenumber q:

$$P_{\delta n_e} = C_n^2 q^{\alpha}, \quad q_0 \leq q \leq q_1 \tag{1}$$

A power-law index of $\alpha = -11/3$ is a prediction of the Kolmogorov theory for density fluctuations in neutral gases. Montgomery, Brown, & Matthaeus (1987) found that a similar spectrum is expected for density fluctuations due to magnetohydrodynamic turbulence in an ionized medium. The coefficient C_n^2 is usually given in units of $\mathrm{m}^{-20/3}$ (m: meters); sometimes the notation $C_{-4} = 10^{-4} C_n^2$ is used. Observations yield $\overline{C_n^2}$, line-of-sight averages of C_n^2, which typically vary between 10^{-4} $\mathrm{m}^{-20/3}$ and 10 $\mathrm{m}^{-20/3}$ for lines of sight in the Galaxy. The more strongly scattered lines of sight, with larger values of $\overline{C_n^2}$, tend to lie at low Galactic latitude toward the inner Galaxy. Values of C_n^2 at particular points, not averaged along lines of sight, may vary by orders of magnitude, as the discussion in § 4 below indicates.

1.2. *Effects of Interstellar Scattering*

Interstellar scattering affects signals from pulsars by temporal broadening, scintillation, and angular broadening (see Rickett 1990 and references therein). Scattering results in propagation along a variety of different ray paths, so that a pulse which left the pulsar at one instant arrives at the observer over an interval τ, the temporal broadening time. Random interference among the different paths produces a diffraction pattern in the plane of the observer. This pattern has a characteristic bandwidth $\Delta\nu$, which is related to temporal broadening τ by an uncertainty principle:

$$2\pi\tau\,\Delta\nu \approx 1 \tag{2}$$

Radiation from the pulsar arrives from a range of angles $\theta \approx (c\tau/d_s)^{1/2}$, the angular size of the pulsar's scattering disk. Here d_s is the characteristic distance from the scattering material to the observer, as discussed further in § 3 below. In general, d_s is a weighted sum of the distances of scattering material along the line of sight. In many respects, the scattering disk may be viewed as a corrupt lens, of aperture θd_s. The spatial resolution of this lens, in the plane of the observer, is $l_d = \lambda/\theta$, where λ is the observing wavelength. As the line of sight moves through the scattering material with velocity $V_\perp$, the diffraction pattern will move across the observer's instrument. The scintillation pattern will thus change on a time scale $t_{\rm ISS} \approx l_d/V_\perp \approx \lambda/(\theta V_\perp)$.

As two antennas are moved apart perpendicular to the line of sight to a scattered pulsar, the signals they receive become uncorrelated as the distance between them approaches the scale of the diffraction pattern, l_d. This decorrelation appears as both amplitude and phase differences between the two signals (Desai et al. 1992). In traditional image synthesis in interferometry, the complex product of signals at the antennas measures one Fourier component of the image of the source. This component corresponds to a wavevector equal to the baseline between the antennas, projected perpendicular to the line of sight (Thompson, Moran, & Swenson 1986). As this projected baseline, B, approaches the scale l_d, the observed decorrelation of the signals indicates structure within the scattered image, on an angular scale of $B/\lambda \lesssim l_d/\lambda$, or a scale of less than or about θ.

If the longest baseline in the antenna network, $B_{\rm max}$, is much less than l_d, all antennas will measure the same signal amplitude and no phase differences. The source will appear unresolved to the network, yielding an upper limit on the angular broadening of $\theta < \lambda/B_{\rm max}$.

If $B_{\rm max}$ is of order or greater than l_d, results of the observation will depend on the time and bandwidth over which the observations are averaged, for a pointlike source such as a pulsar (Cohen & Cronyn 1974). In practice, any measurement of the product of signals at the antennas must average over some time interval T and some bandwidth Δf. If $T < t_{\rm ISS}$ and $\Delta f < \Delta\nu$, the antennas will measure different amplitudes and phases at their points in the diffraction pattern (Desai et al. 1992), but self-calibration will remove those differences and restore the visibility to that of a point source (Cornwell, Anantharamiah, & Narayan 1989). If $T \gg t_{\rm ISS}$ or $\Delta f \gg \Delta\nu$, the product of signals at the two antennas will average over many scintillation patterns, and a smooth decline in visibility with baseline length will be observed (Cohen & Cronyn 1974). The intermediate regime, in which the integration time T is a few times $t_{\rm ISS}$ and the spanned bandwith Δf is a few times $\Delta\nu$, has not been investigated theoretically. We suggest that in this regime the correlation will tend to decline with baseline length, but with large excursions. Because these excursions are due to the incomplete convergence of a sum of several diffraction patterns, self-calibration will not completely remove them.

A "scintle" is the characteristic element of the diffraction pattern of the source, as scattered by the interstellar plasma (Rickett 1988). A scintle extends over an area of $l_d \times l_d$ in the plane of the observer, and over a range of frequency $\Delta\nu$. The time for which an observer samples one scintle is $t_{\rm ISS}$.

The number of scintles sampled by each antenna, N_s, quantifies the extent to which averaging in time and frequency remove the observation from the speckle regime. This number is simply the product of the number of scintillation bandwidths sampled and the number of characteristic time scales sampled. Pulsars with $N_s \leq 1$ are in the speckle regime. In this regime, the intensity fluctuations due to scintillation are exponentially distributed (Scheuer 1968), so that averages over small numbers of scintles will tend to be dominated by a few strong elements. Thus, observations may be expected to depart from the speckle regime only slowly as N_s increases. Estimates based on independent data sets suggest that large averages contain $\sim N_s/5$ effectively independent samples (Cordes 1986).

Refraction by large-scale plasma fluctuations, on scales of order $\theta d_s \approx 10^{13}$ cm, can distort the scattering disk (Rickett, Coles, & Bourgois 1984). Such distortions vary on time scales of $\theta d_s/V_\perp$, or months to years for the scattering disks discussed in this paper. The degree of such distortion depends on the relative strength of large- and small-scale plasma fluctuations. Quantitative searches for refractive effects to date have suggested that they are small, corresponding to a few percent of peak source visibility (Gwinn et al. 1988b; Mutel & Lestrade 1990).

In this paper, we compare measurements of θ with measurements of $\Delta\nu$ and τ to study clumping of scattering material along the lines of sight to 10 pulsars. We report measurements of, or limits on, θ for 10 pulsars, seven of which have not been previously reported. These seven, and pulsar 1933+16 (Gwinn et al. 1988a) were observed in a single VLBI experiment. Measurements of θ for the Crab pulsar, 0531+21 (Mutel et al. 1974; Vandenberg et al. 1976), and the Vela pulsar, 0833−45 (Desai et al. 1992), were obtained from other published VLBI

experiments. Measurements of the diameter of the scattering disk of the Crab pulsar using interplanetary scintillation are consistent with these VLBI measurements (Armstrong & Coles 1978). Eight of the puslars are only moderately scattered. We show that a predominantly uniform medium with a small inhomogeneous component, is to be preferred over a uniform medium or a thin screen alone for these less heavily scattered pulsars. The ninth pulsar, the Crab pulsar, is moderately scattered, but shows time-varying temporal broadening which has been ascribed to its associated supernova remnant, the Crab nebula (Counselman & Rankin 1972). Scattering for this pulsar is consistent with a strong time-variable component near the supernova remnant and a time-constant component distributed uniformly along the line of sight (Vandenberg 1976; Isaacman & Rankin 1977). The 10th pulsar, the Vela pulsar, is heavily scattered. As previously reported by Desai et al. (1992), this strongly scattering material is heavily concentrated near the pulsar, and is associated with the Vela supernova remnant. The observed values of θ and τ for these two pulsars are inconsistent with a uniform scattering medium.

2. COMPARISON OF ANGULAR AND TEMPORAL BROADENING

In this paper, we study the distribution of scattering material along the line of sight by comparing two observables which depend differently on the location of the scattering material: the scintillation bandwidth $\Delta\nu$ or the closely related temporal broadening τ, and the angular broadening θ. This work complements previous studies of the distribution of scattering material, discussed in § 1.1, which has compared scattering among different lines of sight.

2.1. *Location of Scattering Material: the Weighting Function*

The angular broadening θ_H and the temporal broadening τ are both weighted integrals of the strength of scattering along the line of sight, but they are weighted in different ways. Comparison of θ_H and τ thus characterizes the distribution of scattering material along the line of sight. In this section, we compare predictions of simple models for these quantities.

The angular variance of rays from the pulsar at the observer, θ, is given by the expression (Alcock & Hatchett 1978; Blandford & Narayan 1985):

$$\theta^2 = \frac{1}{D^2}\int_0^D dz z^2 \psi(z) \tag{3}$$

where $\psi(z)$ is the mean scattering rate per unit length, and z is the length coordinate along the line of sight from the pulsar at $z = 0$ to the observer at $z = D$. The strength of scattering ψ is a diffusion coefficient. It is related to the coefficient C_n^2 of the spatial spectrum of density fluctuations. The detailed relationship between ψ and C_n^2 depends on the small- and large-wavenumber cutoffs, q_0, q_1, as well as the index α and the distribution of scattering material (see Cordes et al. 1985). We measure θ_H, the FWHM diameter of the scattering disk; it is related to the angular variance θ by

$$\theta_H = \sqrt{4\ln 2}\,\theta\,. \tag{4}$$

The mean excess propagation time is (Blandford & Narayan 1985):

$$\tau = \frac{1}{2cD}\int_0^D dz z(D - z)\psi(z)\,. \tag{5}$$

In practice, the $1/e$ time, rather than the mean time, for temporal broadening is measured, but the difference is small. As noted above, the temporal broadening τ is related to the decorrelation bandwidth $\Delta\nu$ by the uncertainty relation $2\pi\tau\,\Delta\nu = 1$.

A weighting function, $w(z)$, can express the relative effects of scattering material at different positions z along the line of sight for the observables τ (or equivalently $\Delta\nu$) and θ. Such a function characterizes the weighting in equations (3)–(5). For measurements of the angular broadening θ_H of extragalactic sources, $w(z) = 1$: effects of the scattering material are independent of distance. For angular broadening of galactic sources, $w(z) \propto z^2$. For temporal broadening τ of Galactic sources (or scintillation bandwidth $\Delta\nu$), $w(z) \propto z(1 - z)$. Figure 1 displays the form of $w(z)$ for these three cases.

A uniform distribution of scattering material along the line of sight [$\psi(z)$ = constant] is perhaps the simplest model. In this case, equations (3)–(5) yield for the diameter of the scattering disk estimated from the temporal broadening τ:

$$\theta_\tau = \sqrt{16\ln 2}\left(\frac{c\tau}{D}\right)^{1/2}\,. \tag{6}$$

The ratio of measured to estimated diameter,

$$r = \theta_H/\theta_\tau\,, \tag{7}$$

quantifies the comparison of θ_H and τ. Differences between θ_H and θ_τ can arise from clumping of the scattering material along the line of sight as described by equations (3)–(6), and from errors in the assumed pulsar distance D. Section 4.2 below discusses the accuracy of distance measurements for pulsars in our sample.

2.2. *Models for Distribution of Scattering Material*

Nonuniform distributions of scattering material can produce values of r other than 1. For example, scattering material concentrated into a thin screen along the line of sight can produce any value of r. For such a model, $\psi(z) = \psi_0\delta[z - (D - d_s)]$, where ψ_0 is a constant and δ is the Dirac

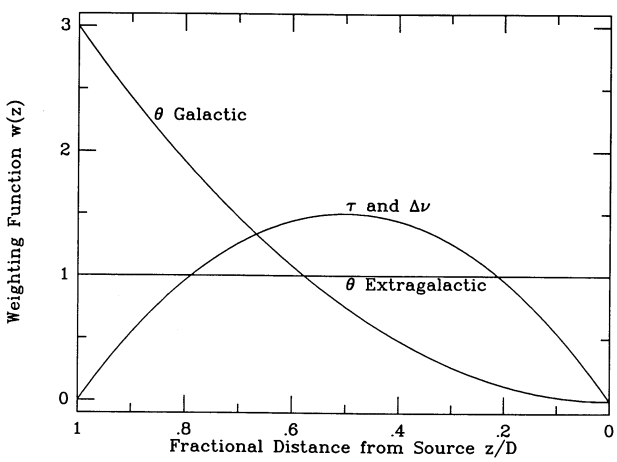

FIG. 1.—Weighting function $w(z)$ for the observables angular broadening θ (for both Galactic and extragalactic sources), and temporal broadening τ (or, equivalently, decorrelation bandwidth $\Delta\nu$), plotted with fractional distance from source, z/D. Note that z runs from source ($z = 0$) to observer ($z = D$). Thus, for Galactic sources, scattering material is most effective in producing angular broadening when it is close to the observer. Scattering material is most effective in producing temporal broadening when it is midway between source and observer. All three curves have been normalized to unit area.

delta function. Note that whereas the coordinate z increases from the pulsar, d_s is the distance of the screen from the observer. In this case, equations (3)–(7) combine to yield:

$$r = \left[\frac{(1 - d_s/D)}{2d_s/D}\right]^{1/2} . \quad (8)$$

Note that, for this model, our r is related to the q of Vandenberg (1976) by $r = (2/q)^{1/2}$. Even in this simpified case, r can vary between 0, for $d_s = D$, and ∞, for $d_s = 0$. This behavior can be understood on quite simple geometric grounds: for a single screen, the maximum temporal broadening (or minimum scintillation bandwidth) results when it is placed midway, whereas the maximum observed scattering angle results when it is very near the observer. An appropriate choice of d_s can thus explain any r.

A somewhat more sophisticated model is a scattering screen of thickness ΔD at a distance d_s from the pulsar [$\psi(z) =$ constant for $(D - d_s) - \Delta D/2 \leq z \leq (D - d_s) + \Delta D/2$; $\psi(z) = 0$ otherwise]. In this case, equations (3)–(7) combine to yield

$$r = \left[\frac{12(1 - d_s/D)^2 + (\Delta D/D)^2}{24(d_s/D)(1 - d_s/D) - 2(\Delta D/D)^2}\right]^{1/2} . \quad (9)$$

We recover the uniform-medium case, $r = 1$, for $d_s = D/2$ and $\Delta D = D$. We recover a thin screen, equation (9), for $\Delta D \ll D$. Much more sophisticated models can be constructed, such as combinations of scattering screens of various thicknesses with a uniform background.

Perhaps a more realistic model includes scattering by both a uniform medium along the line of sight and a single thin screen. For such a model,

$$r = \left[\frac{1 + 3(1 - d_s/D)^2(\psi_1/D\psi_0)}{1 + 6(d_s/D)(1 - d_s/D)(\psi_1/D\psi_0)}\right]^{1/2} . \quad (10)$$

Here ψ_1 parameterizes the strength of scattering of a thin screen. The analogous quantity for the uniform medium is $D\psi_0$. For $\psi_1 \ll D\psi_0$ we recover $r = 1$, the uniform medium value. For $\psi_1 \gg D\psi_0$ we recover equation (8), appropriate for a thin screen alone. Figure 2 shows r as a function of d_s/D for several values of the ratios of strength of thin screen to uniform medium, $\psi_1/D\psi_0$. Deviation of r from 1 increases with the strength of scattering in the single screen, ψ_1. In practice we might expect several concentrations of scattering material along the line of sight, of varying strength. However, if the more strongly scattering screens are relatively much less common, the one most strongly scattering screen along the line of sight may dominate.

3. OBSERVATIONS AND DATA REDUCTION

3.1. *Observations*

Table 1 lists the eight pulsars we observed, with values for their scintillation bandwidths $\Delta\nu$, decorrelation times t_{ISS}, numbers of scintles per integration time and bandwidth N_s, and solar elongation. We observed the pulsars with the Mark II VLBI system with a 2 MHz bandwidth, from 326 to 328 MHz. The observations were made on 1986 March 23 with the radio telescopes at Westerbork (phased array), Jodrell Bank (76 m), Arecibo (305 m), Haystack (46 m), Maryland Point (26 m), Green Bank (43 m), Fort Davis (26 m), and Owens Valley (40 m). We recorded left-circular polarization at all stations with the exception of Arecibo, which has only a linearly polarized feed at these frequencies. We recorded pulsar pulse

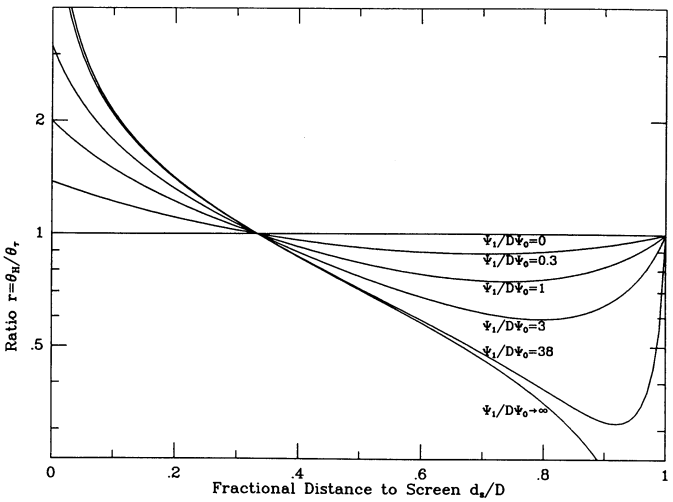

FIG. 2.—The ratio r for a combined uniform medium and single thin screen, plotted with normalized distance to the screen, d_s/D, for several relative strengths of screen and medium, $\psi_1/D\psi_0$. The ratio r is the quotient of observed angular broadening, θ_H; and angular broadening estimated from observed temporal broadening, θ_τ. If the single screen is much weaker than the uniform medium ($\psi_1/D\psi_0 \to 0$), then $r = 1$. If the single screen is much stronger ($\psi_1/\psi_0 D \to \infty$), then r can vary between 0 and ∞, depending on the location of the screen d_s. Note that $d_s = 0$ for a screen at the observer, and $d_s = D$ for a screen at the source.

phase and period information onto the Mark II cassette at the Green Bank telescope at the time of observations. The Mark II correlator in Charlottesville, Virginia, of the National Radio Astronomy Observatory[1] used this information to inhibit correlation when the pulsar was "off," increasing the signal-to-noise ratio by a factor of 2–5 (Gwinn et al. 1986). Data on the Westerbork-Owens Valley baseline showed anomalously high error rates at times, possibly due in part to the effects of this gating. This baseline was not included in our analysis. We coherently averaged the data for 32 s. We found that the coherence time was longer than 100 s. The solar elongations of the pulsars, as given in Table 1, were large enough that the contribution to scattering by the solar wind should be negligible. For each source, we thus obtained series of complex cross-correlation coefficients for each baseline, over the time that the telescope network observed.

3.2. *Data Reduction: Model Fitting*

We reduced the data with the least-square–fit self-calibration technique described by Gwinn et al. (1988a). This technique fits a parameterized model, including both source and instrumental parameters, to the observed correlation coefficients, by minimizing the squared magnitude of the difference of observed and model correlation coefficients. With such an approach, statistics of the observables, the correlation coefficients, are treated correctly, so that the statistical errors of the fit reflect the scatter of data from the various baselines. It also has the advantage that source and instrumental parameters are varied simultaneously, so that the solution and standard errors reflect the covariances among the fitted parameters. Because our model is nonlinear, as discussed below, the fit must be nonlinear as well.

[1] The National Radio Astronomy Observatory is operated by Associated Universities, Inc., under a cooperative agreement with the National Science Foundation.

TABLE 1

OBSERVED PULSARS

Pulsar	Solar Elongation During Observations	Decorrelation Bandwidth[a] $\Delta\nu$ (kHz)	Decorrelation Time[b] t_{iss} (s)	Number of Scintles Averaged[c] N_s
1642−03.....	111°	15	45	130
1818−04.....	87	0.072	5.5	1.6×10^5
1919+21.....	73	180	150	11
1929+10.....	69	990	350	2
1933+16.....	69	0.18	8.5	4.2×10^4
1937+21.....	68	1.2	70	1.7×10^3
2016+28.....	61	46	470	40
2020+28.....	61	100	290	20

[a] See Table 5 for references (Temporal Broadening).
[b] From Cordes 1986.
[c] Number of scintles = $N_s = (2\ \mathrm{MHz}/\Delta\nu) \times (32\ \mathrm{s}/t_{iss})$, where each pair of parentheses is set to 1, if the expression within the parentheses is less than 1.

The model, $C_{AB}(t)$, for the observed correlation coefficient between stations A and B, is given by the expression:

$$C_{AB} = \Gamma_A \Gamma_B \exp\left[\imath\phi_B - \imath\phi_A\right] S V_{AB} . \quad (11)$$

In this expression, the gains of the two stations are Γ_A and Γ_B, including effective area of the antenna and system temperature. Phases associated with the stations, as introduced by instrumental and propagation effects, are ϕ_A and ϕ_B. The interferometric visibility, normalized by the flux density of the source, is V_{AB}. The flux density S times this visibility is one component of the Fourier transform of the image of the source, in correlator units. In general, all of these quantities may vary with time. In particular, the large pulse-to-pulse variations in pulse intensity expected for pulsars will cause S to vary significantly.

As discussed below, we let the parameters for station gains Γ and station phases ϕ vary with time, except in cases where the signal-to-noise ratio was too low to allow determination of the gain parameters in a single 32 s integration. In such cases, we determined single values of Γ for each antenna for each pulsar. The value of Γ is expected to vary among the pulsars because of the differing contribution of extended emission to the system temperature at the position of the pulsar, and the different beam widths of the antennas.

We model the visibility on the baseline between antennas A and B as a nearly Gaussian function of the projected baseline length, B_{AB}, measured in observing wavelengths:

$$V_{AB} = \exp\left[-\frac{1}{2}\left(\frac{\pi^2}{2\ln 2}\,\theta_H^2\, B_{AB}^2\right)^{(\alpha_{vis}-2)/2}\right], \quad (12)$$

In terms of the traditional components of projected baseline u and v, $B_{AB} = (u^2 + v^2)^{1/2}$. If the index α_{vis} is set to 4, the visibility becomes a circular Gaussian distribution, with θ_H its FWHM diameter. In practice, we fitted for the parameter $[\theta_H^2]$ rather than θ_H; because the model visibility can increase with baseline length for $[\theta_H^2] < 0$, this parameter converges more quickly and reliably near 0. Our (u, v) coverage was poor and largely extended in an east-west direction; it was not diverse enough to support models including parameters for elongation of the scattering disk. Except for pulsar 1933+16, we did not solve for α_{vis}, but tried solutions with both $\alpha_{vis} = 4$ and the Kolmogorov index of $\alpha_{vis} = 11/3$; the resulting values of θ_H differed by much less than their uncertainties from other factors.

The data are complex quantities; the model, given by equation (12), is real. The imaginary parts of the data, after fitting for station phases ϕ_A and ϕ_B, are expected to vary from zero only due to noise. Unlike a fit to the amplitude of the correlation function, a fit to the complex visibility is not subject to noise bias. Such as would arise on our longer baselines, where correlated flux density is low and noise can dominate the amplitude of the correlation function (Thompson et al. 1986). Likewise, it is not subject to the bias introduced by refractive modulation of the scattering disk, due to density irregularities just smaller than the scattering disk (Narayan & Goodman 1989). In practice, fitting of equation (3) to data involving stations with few partners, or low signal-to-noise ratio to all partners, can align the phases of the noise and eliminate these advantages. As discussed in the following section, we eliminated such data from our fit.

Because our procedure is similar to traditional self-calibration, we expect that it will yield unit visibility on all baselines, for pulsars observed in the speckle regime of interstellar scattering. As Table 1 shows, none of our observations are in the speckle regime, but 4 approach it to within a factor of 50, and 1 to within a factor of 2. We expect that such observations may show some character of the speckle regime, because the expected distribution function of scintles with intensity is an exponential. Thus a few strong scintles will tend to dominate any average.

TABLE 2

OBSERVED SIZES OF PULSARS' SCATTERING DISKS

Pulsar	Fitted Parameter $[\theta_H^2]$ (mas^2)	Notes	Scattering Disk Diameter θ_H (mas)
1642−03.....	44.5 ± 15.2	...	6.7 ± 1.1
1818−04.....	4165 ± 1209	...	64.5 ± 9.4
1919+21.....	20.6 ± 13.2	[a]	4.5 ± 1.3
1929+10.....	−2.5 ± 8.4	[a]	<2.4
1933+16.....	230.4 ± 38.2	[b]	15.2 ± 1.3
1937+21.....	214.1 ± 55.7	...	14.6 ± 1.9
2016+28.....	−8.0 ± 37.9	[a]	<5.5
2020+28.....	25.4 ± 17.1	[a]	5.0 ± 1.6

[a] Observation approaches snapshot regime; see Table 1.
[b] Uncertainty estimated from statistical uncertainty from fits (±0.6 mas) in quadrature with difference between values for $\alpha_{vis} = 3.67$ and $\alpha_{vis} = 4.00$ (±1.0 mas). Result differs slightly from Gwinn et al. 1988a because here station gains Γ were allowed to vary with time.

3.3. *Results of Model Fitting*

We applied the model described by equations (11) and (12) to the data. Table 2 summarizes results of model fitting, and Figure 3 shows self-calibrated data and best-fitting models for the eight pulsars observed in 1988 March. To show relative uncertainties of the visibilities for different baseline lengths, the data have been binned in baseline length, and the mean real and imaginary parts plotted for each bin. The standard deviations of these means are also plotted. The best-fitting models are shown.

The four pulsars more than a factor of 50 from the speckle regime (1642−03, 1818−04, 1933+16, and 1937+21) show significant declines in visibility with baseline length, as Figure 3 and Table 2 show. Pulsars 1642−03 and 1818−04 are at such low declination that they could not be observed at Arecibo and were not visible at both ends of the longest baselines simultaneously. Thus only shorter baselines yielded data. For pulsar 1818−04, which is heavily resolved, we include in the fit only antennas for which the source was detected on at least one baseline. Antennas so isolated that all baselines to them were long enough to resolve the source also produced useful information, in the form of upper limits. However, inclusion of these data in the fit confused gain and phase self-calibration, so they were not included in the fit and are not shown in Figure 3. Pulsar 1937+21 had a period too short to be accommodated by our gating system. The data have correspondingly lower signal-to-noise ratio. We solved for time-independent gains Γ

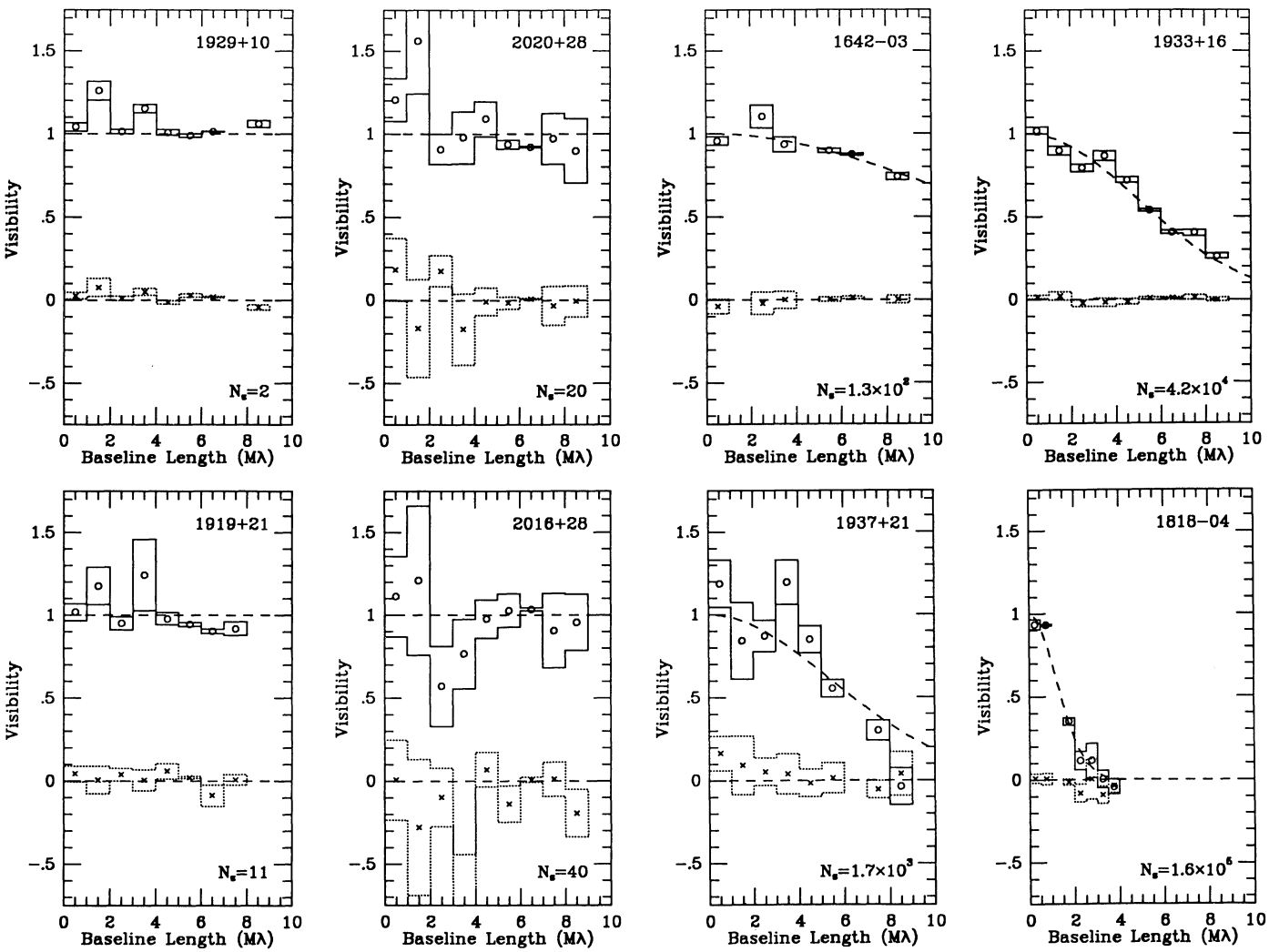

FIG. 3.—Distribution of visibility with baseline length for eight pulsars observed at 326 MHz, after self-calibration. The real and imaginary parts of the visibility were binned by baseline length, and the mean and standard deviation of the mean determined for each bin. Circles show the mean real part; crosses show the mean imaginary part. Boxes about the points show standard deviation of the means. The data were weighted by the gains of the antennas in calculating these quantities. The plots are arranged by the number of scintles averaged per integration time and bandwidth, N_s, as described in the text. The model visibility for a point source is shown for pulsars close to the speckle regime ($N_s < 50$: pulsars 1929+10, 1919+21, 2020+28, and 2016+28). Pulsars 1929+10 and 1919+21 are closest to the speckle regime; their nearly unit, real visibilities may reflect either small angular broadening or the effects of self-calibration. Pulsars 2020+28 and 2016+28 are in an intermediate regime, where observations average over too few scintles to produce a smooth scattering disk, but self-calibration does not remove effects of scattering. The best-fitting model visibility is shown for pulsars further from the speckle regime ($N_s > 50$: pulsars 1642−03, 1937+21, 1933+16, and 1818−04). Smooth declines of visibility with baseline length describe data for these pulsars. Because of the rapid decline of visibility for pulsar 1818−04, we used bins half as wide as those for the other pulsars. Pulsar 1937+21 had a pulse period too short for our gating system, and so yielded lower signal-to-noise ratio data than the other pulsars.

for each antenna for this pulsar, but we allowed the model flux density, S, to vary with time.

Our observations of four pulsars (1919+21, 1929+10, 2016+28, and 2020+28) approach the speckle regime. As Table 2 indicates, fits to all of these pulsars yielded values of θ_H consistent with 0. This is perhaps not surprising, as the small numbers of scintles N_s, given in Table 1, result from large decorrelation bandwidths $\Delta\nu$, or equivalently from little temporal broadening τ. For small τ, one expects $\theta \approx (c\tau/d_s)^{1/2}$ to be small. We also expect to measure $\theta_H = 0$ for pulsars in the speckle regime, independent of their angular scattering, due to the effects of self-calibration. Thus, interpretation of the fitted angular broadening is ambiguous.

Pulsars 1919+21 and 1929+10 approach the speckle regime most closely, as Table 1 indicates. Their visibilities follow the behavior expected for point sources well. This agreement could indicate that the scattering disks of these pulsars are indeed pointlike to our VLBI network or it could simply reflect the fact that the observations sample a small number of scintles, and self-calibration removes the amplitude and phase fluctuations.

Pulsars 2016+28 and 2020+28 also yield values of θ_H consistent with zero, but their visibilities vary around the behavior expected for point sources much more than those of pulsars 1919+21 and 1929+10. We suggest that the diffraction patterns of these two pulsars vary across our network, so that $B_{\max} > l_d$, but that self-calibration cannot remove these variations, because they represent averages over several scintles. These pulsars show the large variations in visibility expected for the intermediate regime between the speckle regime ($N_s \leq 1$), for which self-calibration restores unit visibility; and the average regime ($N_s \gtrsim 50$), for which visibility decreases smoothly with baseline length.

3.4. *Diameters of Pulsars' Scattering Disks from the Literature*

Interferometric measurements of the angular broadening of pulsars have been published for pulsar 0531+21, the Crab pulsar (Mutel et al. 1974; Vandenberg et al. 1976; Vandenberg 1976); and for pulsar 0833−45, the Vela pulsar (Desai et al. 1992). Table 3 lists these measurements and compares them with contemporaneous measurements of temporal broadening.

Because the Crab pulsar is not heavily scattered, measurements of the angular diameter of its scattering disk must be made at observing wavelengths $\lambda \gtrsim 2$ m, where the scattering disk is large. Counselman & Rankin (1972) noted that the Crab pulsar shows marked variations of τ with time; they concluded that the Crab Nebula, the supernova remnant associated with and surrounding the pulsar, is responsible for the variable part of the scattering. Lyne & Thorne (1975) noted that the temporal broadening of the Crab pulsar increased dramatically over a period of a few weeks. They suggested that occultation by a localized plasma irregularly produced this event. Vandenberg et al. (1976) measured the angular diameter θ_H at two times, when τ had different values. They found that θ_H remained constant while τ varied. As Vandenberg (1976) noted, this indicates that the time-variable part of the scattering is quite close to the pulsar, as discussed in § 3 below. Mutel et al. (1974) also measured the angular diameter of the pulsar with VLBI, at lower frequency. They do not present a value for τ, but Isaacman & Rankin (1977) present contemporaneous measurements and a scaling law from which τ at the observing frequency can be calculated. Results of Mutel et al. and Isaacman & Rankin agree well with those of Vandenberg et al., at the earlier of Vandenberg et al.'s epochs. The diameter of the pulsar has also been measured by interplanetary scintillation (IPS), with results in agreement with those of these two groups (Armstrong & Coles 1978 and references therein).

Isaacman & Rankin were able to distinguish two characteristic times in their pulse broadening measurements: a short time scale of $\approx$2.5 ms at an observing frequency of 100 MHz, and a longer, variable time scale of $\approx$10 to 20 ms. They associated the short time scale with scattering in the interstellar medium and the longer time scale with scattering in the Crab supernova remnant. We treat the two time scales separately in comparisons of θ_H and τ, in § 4 below.

Desai et al. (1992) inferred the diameter of the Vela pulsar's scattering disk from the observed phase variation on short VLBI baselines, in the speckle regime. They also measured the decorrelation bandwidth, $\Delta\nu$, from the same series of observations. Equation (2) then yields the temporal broadening τ. Table 3 gives the results. As discussed further below, Desai et al. concluded that the scattering material, as observed via both θ_H and τ, lies close to the pulsar.

4. COMPARISON OF MEASUREMENTS

4.1. *Comparison of θ_H and τ for Pulsars in Our Sample*

The pulsars in our sample lie at low Galactic latitude (except for pulsar 1642−03) and are moderately scattered (except for pulsar 0833−45). Table 4 give the galactic coordinates and strength of scattering for pulsars in our sample. Table 5 gives values of τ from published measurements of τ or $\Delta\nu$ at frequencies near 326 MHz, estimates of distance D, and the corresponding values of θ_τ. For pulsars 0531+21 and 0833−45, results from Table 4 have been scaled to 326 MHz using the scaling relationships $\theta_H \propto \lambda^{\alpha/(\alpha-2)}$ and $\tau \propto \lambda^{2\alpha/(\alpha-2)}$ (Lee & Jokipii 1976), where we expect $\alpha = 3.7$ for the pulsar 0531+21 (Isaacman & Rankin 1977) and $\alpha = 4.0$ for the pulsar 0833−45

TABLE 3

SIZES OF PULSARS' SCATTERING DISKS FROM THE LITERATURE

Pulsar	Observing Frequency (MHz)	Measured Diameter θ_H (mas)	Temporal Broadening τ (ms)	Epoch of Observations	References
0531+21.....	111.5	70 ± 10	15 ± 3	1971 −1972	1
0531+21.....	111.5	70 ± 10	25 ± 5	1972 −1973	1
0531+21.....	26.3	1300 (+230, −130)	7500 (+2100, −1400)[a]	1973.0–1973.2	2
0833+45.....	2291	1.6 ± 0.2	0.0023 ± 0.0002	1991.2	3

[a] From Isaacman & Rankin 1977, scaled with their relation $\tau \propto f^{-4.4}$ to the 26.3 MHz observing frequency of Mutel et al. 1974.

REFERENCES.—(1) Vandenberg et al. 1976; (2) Mutel et al. 1974; (3) Desai et al. 1992.

TABLE 4

DISTRIBUTION OF PULSARS

Pulsar	Galactic Longitude l^{II}	Galactic Latitude b^{II}	Strength of Scattering[a] $\log_{10} \overline{C_n^2}$
0531+21c	184°.6	−5°.8	−3.60[b]
0531+21v			−3.0 to −2.6[c]
0833−45	263.6	−2.8	0.16
1642−03	14.1	26.1	−3.37
1818−04	25.5	4.7	−2.05
1919+21	55.8	3.5	−2.29
1929+10	47.4	−3.9	−1.97
1933+16	52.4	−2.1	−2.73
1937+21	57.5	−0.3	−3.49[d]
2016+28	68.1	−4.0	−3.48
2020+28	68.9	−4.7	−3.60

[a] From Cordes et al. (1985), except for 0531+21 and 1937+21.

[b] Includes only the time-constant part of interstellar scattering (from Vandenberg 1976; Isaacman & Rankin 1977; & Cordes et al 1985).

[c] Range for the time-varying part of interstellar scattering (from Isaacman & Rankin 1977). Note that the actual value of C_n^2 is probably much greater, since the time-varying part of the scattering is concentrated near the pulsar.

[d] From Cordes 1986.

(Backer 1974). We treat the time-varying and time-constant parts of the temporal broadening separately for pulsar 0531+21, indicated by entries 0531+21v and 0531+21c. Figure 4 compares these values of θ_τ with our measured diameters θ_H. Table 5 also gives the ratios of measured to estimated diameter, r, as discussed in § 2. As Figure 3 shows, we obtain values of r that are consistent with 1, to within a factor of $2^{1/2}$ for eight of the 10 pulsars. The two exceptions are pulsar 0531+21v, for which angular broadening θ_H is compared with the time-varying part of temporal broadening τ; and pulsar 0833−45. Both of these pulsars lie within remnants of the

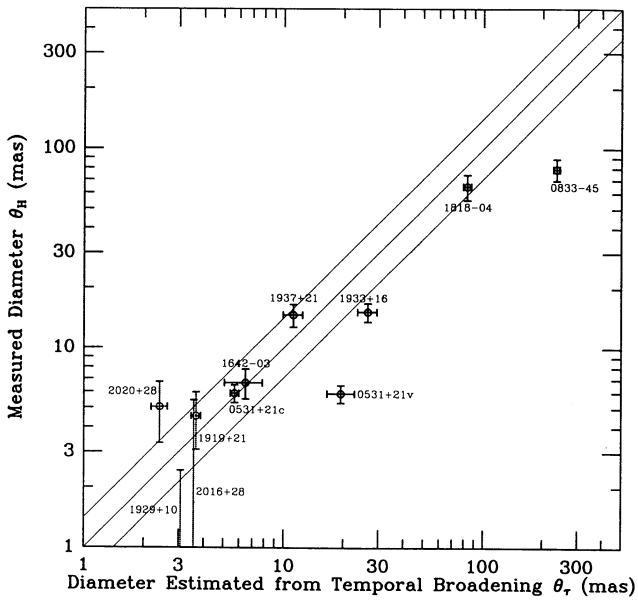

FIG. 4.—Diameters of the scattering disks of 10 pulsars, θ_H, plotted with the diameter as estimated from the temporal broadening of pulses, θ_τ. Agreement of θ_H and θ_τ is expected for a uniform distribution of scattering material. Pulsar 0531+21 is shown both as 0531+21v, with θ_τ estimated from the component of its temporal broadening that varies with time; and as 0531+21c, with θ_τ estimated from the component that is constant in time. Measurements for pulsars observed close to the speckle regime are shown dotted. Measured sizes may depend on factors besides the angular broadening for these objects, as discussed in the text. Distances of the pulsars are probably accurate to no better than a factor of 2, leading to an expected error in θ_τ of about a factor of $2^{1/2}$. Agreement of θ_H and θ_τ is good to about this factor of $2^{1/2}$, except for pulsars 0531+21 and 0833−45, which are heavily scattered by the supernova remnants in which they lie. This agreement suggests that scattering material is uniformly distributed along moderately scattered lines of sight.

TABLE 5

COMPARISON OF ANGULAR BROADENING AND SCINTILLATION DATA

Pulsar	Angular Diameter θ_H (mas)	Temporal Broadening from Scintillation τ (μs) at 326 MHz	Temporal Broadening Reference	Dispersion Based Distance[a] (kpc)	Annual Parallax or H I Absorption Distance[b] (kpc)	Adopted Distance D (kpc)	Diameter Estimated from Scintillations θ_τ (mas)	Radio $r = \theta_H/\theta_\tau$
0531+21c	5.9 ± 0.6[c]	14 ± 2[c]	[d]	2.0	2.0 ± 0.5	2.0	5.7 ± 0.3	1.03 ± 0.14
0531+21v	...	40 to 200[c]	[e]				16.6 to 23	0.31 to 0.29
0833−45	79 ± 10[c]	5800 ± 400[c]	[f]	0.5	0.5 ± 0.1	0.5	235 ± 9	0.34 ± 0.04
1642−03	6.7 ± 1.1	11 ± 5	[g]	1.3		1.3	6.5 ± 1.4	1.03 ± 0.29
1818−04	64.5 ± 9.4	2200 ± 200	[h]	2.7	<1.6 ± 0.5	1.5	83 ± 3.8	0.78 ± 0.12
1919+21	4.5 ± 1.3	0.91 ± 0.10	[i]	0.32	<2.8 ± 1.2	0.32	3.7 ± 0.2	1.24 ± 0.40
1929+10	<2.4	0.16 ± 0.06	[i]	0.08	<1.6 ± 0.5	0.08	3.1 ± 0.6	<0.79
1933+16	15.2 ± 1.3	900 ± 200	[g]	4.6	>5.2 ± 1.7	6.0	27 ± 3	0.57 ± 0.08
1937+21	14.6 ± 1.9	133 ± 30	[j]	1.7	>4.6 ± 1.9, <14.8 ± 0.9	5.0	11.2 ± 1.3	1.31 ± 0.32
2016+28	<5.5	3.5 ± 0.6	[i]	0.4	>3.2 ± 2.1	1.3	3.6 ± 0.3	<1.54
2020+28	5.0 ± 1.7	1.6 ± 0.3	[i]	0.7	>3.1 ± 2.1	1.3	2.4 ± 0.2	2.09 ± 0.73

[a] Calculated using the model of Lyne, Manchester, & Taylor 1985.

[b] From Frail & Weisberg 1990.

[c] Scaled to 326 MHz using the scaling laws, with frequency f, for angular broadening $\theta_H \propto f^{-\alpha/(\alpha-2)}$ and for temporal broadening $\tau \propto f^{-2\alpha/(\alpha-2)}$ (Lee & Jokipii 1976). We adopt $\alpha = 3.7$ for pulsar 0531+21 (Isaacman & Rankin 1977), and we adopt $\alpha = 4.0$ for pulsar 0833−45 (Backer 1974).

[d] Time-constant part of the temporal broadening (Isaacman & Rankin 1977). Isaacman & Rankin resolve the temporal broadening into a larger component that varies with time, and a smaller one that does not.

[e] Time-varying component of the temporal broadening, during the size measurements in Table 3. From Isaacman & Rankin (1977) and Vandenberg 1976.

[f] Desai et al 1992.

[g] Cordes et al 1985.

[h] Alurkar, Slee, & Bobra 1986.

[i] Cordes 1986.

[j] Rawley, Taylor, & Davis 1988.

supernovae in which they formed; these remnants are responsible for most of the temporal broadening (Vandenberg 1976; Desai et al 1992). Pulsar 0531+21 yields a ratio r consistent with 1 when θ_H is compared with only the time-constant part of temporal broadening (0531+21c). Our results are thus consistent with $r = 1$ for the distributed component of interstellar scattering along our lines of sight.

4.2. *Distance Estimates*

Differences between θ_H and θ_τ can arise from errors in the assumed pulsar distance D, as well as from clumping of the scattering material along the line of sight as discussed in § 2. Comparisons with trigonometric parallaxes (Gwinn et al 1986 and references therein) and kinematic distances from H I absorption spectra (Frail & Weisberg 1990 and references therein) show that pulsar distances estimated from models for the interstellar free electron density and the resulting observed pulse dispersion are accurate to about a factor of 2 in most cases (Lyne, Manchester, & Taylor 1985; Frail & Weisberg 1990). H I absorption data have been published for all pulsars in our sample, yielding kinematic distances or upper or lower limits on them as summarized in Table 3. Trigonometric distance measurements have been published for two of the pulsars we observed. For pulsar 1929+10, Salter, Lyne, & Anderson (1979) found an annual parallax of 22 ± 8 mas, corresponding to $D = 0.045^{+0.026}_{-0.012}$ kpc; however, Backer & Sramek (1982) placed an upper limit of 4 mas on its annual parallax, corresponding to $D > 0.25$ kpc, inconsistent with the value given by Salter et al. The dispersion-based distance of 0.08 kpc is within a factor of 3 of both parallax results. Pulse timing of pulsar 1937+21 has yielded a lower limit on its distance of 2.5 kpc (Rawley, Taylor, & Davis 1988), consistent with the H I distance but not the dispersion-based distance. Because the various measures of distance agree to no better than a factor of 2, distance errors are probably responsible for $\sim 2^{1/2}$ of the scatter of the observed ratios.

4.3. *Three Groups of Pulsar*

Based on values for r and N_s, we can divide the pulsars in our sample into three groups: lightly scattered pulsars close to the speckle regime; pulsars moderately scattered by the interstellar plasma; and young pulsars strongly scattered by their surrounding, associated supernova remnants.

The first group, the four pulsars close to the speckle regime, consists of 1919+21, 1929+10, 2016+28, and 2020+28. These pulsars are close enough to the speckle regime that the interpretation of our fitted values for θ_H is uncertain, although pulsars 2016+28 and 2020+28 show indications that the spatial scale of the diffraction pattern is shorter than our longest baseline, $\sim 9 \times 10^6 \lambda$: $l_d < B_{\max}$. We then might expect $\theta_H \gtrsim 5$ mas.

The second group contains pulsars 1642−03, 1818−04, 1933+16, and 1937+21. These pulsars are moderately scattered by material along the line of sight. We may also include 0531+21c in this group, where we use the time-constant component of the temporal broadening, τ, with the measured angular broadening, θ_H, to compute r. This value of r reflects the extended component of scattering along the line of sight to 0531+21. All these pulsars show values of r close to 1. These values suggest that the scattering material is relatively uniformly distributed along the line of sight, as it is quite improbable that pulsars with such a variety of distances would all tend to have scattering material concentrated near $d_s = \frac{1}{3}D$, or other distributions that would produce the same result for r.

Pulsars 0531+21 and 0833−45 form a third group. Values of r are significantly less than 1 for both pulsars. Both pulsars are young and lie within remnants of the supernovae in which they formed. These small values of r arise from concentration of scattering material at these remnants, close to the pulsars.

5. DISCUSSION

5.1. *Moderately Scattered Lines of Sight*

Our results suggest that the scattering material is nearly uniformly distributed along lines of sight a few kiloparsecs long. This conclusion is clearest for pulsars in the second group of the previous section: pulsars 1642−03, 1818−04, 1933+16, 1937+21, and 0531+21c, (for which we include only the time-constant component of scattering). Values of r are consistent with 1.0 to within 1 σ for two of these pulsars, and within 2 σ for four. This is somewhat better agreement than expected even if the scattering material is uniform, because distance estimates for the pulsars are probably accurate to only a factor of 2, as discussed in § 3.1. Distance errors should thus produce an additional scatter of a factor of $2^{1/2}$ in estimated values for r, beyond that included in the quoted standard errors in Table 5.

For pulsar 1933+16, r is 0.57 ± 0.08, just more than a factor of $2^{1/2}$ less than 1. This discrepancy is unlikely to be due to the estimated distance of the pulsar. To bring r to unity, the pulsar would have to lie 21 kpc from Earth, rather than 6 kpc. It would then lie 17 kpc from the Galactic center, further than any other known pulsar (Lyne, Manchester, & Taylor 1985). (Here we take the distance to the Galactic center to be $R_0 = 10$ kpc, in accordance with Lyne et al. and with Frail & Weisberg, although R_0 is probably closer to 8.5 kpc; see Gwinn, Moran, & Reid 1992). H I absorption measurements, summarized in Table 5, yield only a lower limit on the distance to the pulsar. The dispersion-based distance estimate is 4.6 kpc. Thus, the small value of r probably reflects concentration of scattering material close to the pulsar.

The line of sight to pulsar 1933+16 may intercept the Strömgren sphere around Wolf-Rayet star 93 (Prentice & ter Haar 1969). This star lies less than 3° from the line of sight to the pulsar, and ~ 2 kpc from Earth. Enhanced scattering might be expected near the edge of this Strömgren sphere; the edge is too close to Earth to explain the small value of r unless the pulsar lies at the near end of the range of possible distances.

Pulsar 1642−03 is another possible exception. This pulsar lies behind the H II region surrounding ζ Oph (Prentice & ter Haar 1969), which might be expected to act as a thin screen of strong density fluctuations. This H II region is at a distance of 0.17 kpc, whereas the dispersion-based distance for the pulsar is 1.3 kpc. However, Graham et al. (1974) suggest, on the basis of H I absorption measurements, that the pulsar is at a distance of between 0.15 and 0.17 kpc; moreover, they suggest that the H II region could be responsible for all the observed pulse dispersion. Applying equation (9), we find that our observations are consistent with either the dispersion-based distance and uniformly distributed scattering material, or the closer pulsar distance and scattering material concentrated near the pulsar, in the H II region. Resolution of this ambiguity will require further work; in particular, if the pulsar is indeed at the closer distance, it is one of the closest pulsars and its trigonometric parallax should be measurable.

Predictions of r for the thin-screen and extended-medium

models discussed in § 2.1 provide an interesting comparison with observations of the five moderately scattered pulsars. The value of r for pulsar 1933+16 rules out a purely uniform medium along the line of sight. If the scattering material is concentrated in a single screen along each line of sight, the probability that $0.57 < r < 1.31$ for five pulsars, as observed, is less than 1%, if the screens are placed randomly along the lines of sight. The medium must contain both localized and distributed components. If we model the localized component as a single screen, placed randomly along the line of sight, and the distributed component as a uniform medium, we can use equation (10) to set limits on their relative strengths of scattering. As Figure 3 suggests, the strength of scattering in the thin screen, ψ_1, must be at least 3 times that of the uniform medium, $D\psi_0$, to obtain $r = 0.57$, as observed for pulsar 1933+16. If we suppose that the same ratio of strengths $\psi_1/D\psi_0$ characterizes all five lines of sight, we can set limits on $\psi_1/D\psi_0$. The preferred value is $\psi_1/D\psi_0 = 3$, with a 65% confidence interval of $1.9 \leq \psi_1/D\psi_0 \leq 3.7$, and a 95% confidence interval of $1.1 \leq \psi_1/D\psi_0 \leq 9$. In fact, the medium is likely to be somewhat more uniform than this analysis suggests, because distance errors will increase the scatter of r.

The lines of sight to moderately scattered pulsars in our sample are 1.3–6 kpc long. The two longest lines of sight, to pulsars 1933+16 and 1937+21, show values of r most discrepant from unity. However, the strongest scattering, and largest values of C_n^2, are along the lines of sight to pulsars 1642−03 and 1818−04, as Table 4 shows. In their survey of scattering in the first quadrant of the Milky Way, Fey et al. (1991) found weaker scattering in the interarm region near Galactic longitude 60°, where pulsars 1933+16 and 1937+21 lie, than at nearby longitudes. Pulsars 1642−03 and 1818−04 lie near edge of this region of reduced scattering. The differences in C_n^2 among lines of sight with uniformly distributed scattering material suggest that the strength of scattering in the uniform component varies on large scales.

Our observations are in agreement with the spirit of the two-component model discussed in § 1 above, but the lines of sight to pulsars in our sample are shorter and less heavily scattered than the lines of sight used to construct those models. Both Dennison et al. (1984) and Cordes et al. (1985) give quantitative models of the two-component medium, based on their samples of scattered sources. These models predict a significant probability ($P \approx 75\%$) of encountering a strongly scattering cloud only along the line of sight to pulsar 1937+21; other pulsars in our sample are either too close or at too high a Galactic latitude to lie behind such a cloud. However, even a single cloud produces angular broadening greater than $\theta_H \approx 0.23''$ in the Dennison et al. model, and $C_n^2 \approx 10^{-2}$ in the Cordes et al. model. Both are much greater than the scattering observed for the pulsars in our sample. Fey et al. (1991) suggest that strongly scattering clouds are absent in the interarm region; our observations are consistent with this hypothesis. Cordes et al. suggest that the heavily scattering clouds follow a power law, with the largest clouds relatively less common; in this picture our observations probe the smaller, more common clouds.

5.2. *Pulsars within Supernova Remnants*

Pulsars 0531+21 (the Crab pulsar) and 0833−45 (the Vela pulsar) lie within the associated Crab and Vela-X supernova remnants. These pulsars have the smallest values of r of any in our sample, ~0.3. As equation (10) and Figure 2 indicate, such values of r can be obtained only for a strong concentration of scattering material extremely close to the pulsar. For the uniform-medium plus thin-screen model given by equation (10), they require a strength of scattering in the screen, ψ, at least 38 times that of the uniform medium, $D\psi_0$. This scattering material appears to be associated with the enclosing supernova remnant for these two pulsars.

Several groups have identified scattering material along the line of sight to the Crab pulsar with the Crab supernova remnant. Counselman & Rankin (1972) and Isaacman & Rankin (1977) made this identification on the basis of the presence of two characteristic time scales of broadening for the pulsar, one of which varies over periods of months and the other of which remains constant. Lyne & Thorne (1975) reported an episode of particularly heavy broadening, with substantial variations in the shape of the broadening function, lasting a few months. Vandenberg (1976) compared θ and τ in an approach similar to ours.

The strong scattering along the line of sight to the Vela pulsar has been traditionally ascribed to the Gum Nebula (see, for example, Williamson 1974; Cordes et al. 1985). The near side of this nebula lies about halfway to the pulsar (Reynolds 1976). However, Desai et al. (1992) found from comparison of θ and τ that the material lies much closer to the pulsar than the Gum Nebula. They identified the scattering with the Vela-X supernova remnant, which surrounds the pulsar.

Strong scattering by young supernova remnants may be associated with acceleration of cosmic rays. Bell (1978) and Blandford & Ostriker (1978) suggested that Alfvèn waves upstream of a shock, as in a young supernova remnant, mediate particle acceleration. They noted that energetic particles can be reflected repeatedly across the shock front by such waves, which they themselves will generate. These particles will gain energy with each reflection, until they finally escape. The bulk of cosmic-ray acceleration must occur for supernova remnants with sizes between 1 and 50 pc (Blandford & Ostriker 1980; Franson & Epstein 1980).

Altunin (1980) suggested that Alfvèn waves from streaming cosmic rays could excite the plasma fluctuations that cause scintillation. Spangler et al. (1986) suggested that enhanced radio-wave scattering should accompany cosmic-ray acceleration in young supernova remnants. Spangler et al. based their argument on theoretical models for conversion of Alfvèn wave turbulence into density fluctuations, and on observations of density fluctuations associated with shocks in the solar wind. Spangler et al. (1986) and Spangler, Fey, & Cordes (1987) search for enhanced scattering associated with young supernova remnants; their results are discussed in § 5.3 below. Desai et al. (1992) suggested that the strong scattering of the Vela pulsar by the surrounding Vela-X supernova remnants, which they observed, and the scattering of the Crab pulsar by its surrounding remnant, observed by Counselman & Rankin and Vandenberg, are both due to the plasma fluctuations that accompany cosmic-ray acceleration in these remnants.

About eight known pulsars are believed to be still associated with the supernova remnants in which they formed. Temporal broadening has been measured for three of these objects: pulsars 0531+21 and 0833−45, discussed above, and pulsar 1951+32, associated with the supernova remnant CTB 80 (Strom 1987; Kulkarni et al. 1987; Fruchter et al. 1987). Table 6 lists distances and ages of these pulsars, the temporal broadening τ, and the distance of the scattering screen from the

TABLE 6

PULSARS IN SUPERNOVA REMNANTS WITH MEASURED SCATTERING PARAMETERS

Pulsar	Associated Supernova Remnant	Estimated Distance[a] D (kpc)	Timing Age[a] $P/\dot{P}$ [$\log_{10}$ (yr)]	Temporal Broadening at 1 GHz τ (μs)	Distance Scattering Screen from Pulsar ζ (pc)	Index of Density Fluctuations α	Variation of Dispersion Measure Over 1 Year ΔDM (pc cm^{-3})
0531+21v	Crab Nebula	2.00	3.10	0.3 to 1.4[b]	<80[c]	3.7[d]	0.04[d,e]
0833−45	Vela-X	0.50	4.06	66[f]	95 ± 15[f]	4.0[g]	0.06[h]
1951+32	CTB 80	1.30	5.03	0.56[i]	...	...	0.013[j]

[a] Lyne & Smith 1990.
[b] Ranges of values found by Isaacman & Rankin 1977. Lyne & Smith 1975 found $\tau \approx 40.\ \sim \mu$s for a period of a few months. Values scaled to $f = 1$ GHz using $\tau \propto f^{-4.4}$.
[c] See text.
[d] Isaacman & Rankin 1977.
[e] Lyne, Pritchard, & Smith 1988.
[f] Desai et al. 1992.
[g] Backer 1974.
[h] Hamilton, Hall, & Costa 1985.
[i] Adapted from measurements of decorrelation bandwidth by Fruchter et al. 1987.
[j] Foster, Backer & Wolszczan 1990.

pulsar, $\zeta = (D - d_s)$, as determined from the ratio r. For the Crab pulsar, we set limits on ζ from the fact that angular broadening does not change detectably when temporal broadening changes by more than a factor of 2. Table 6 also lists the spectral index of density fluctuations, α, as defined by equation (1). A more negative value of α corresponds to a greater amplitude of large-scale density fluctuations, relative to small-scale ones, for fluctuations on the length scales $l \lesssim 10^{11}$ cm responsible for diffractive scattering.

Table 6 also lists the variation in dispersion measure DM, over a period of a year. Dispersion measure is the column density of electrons toward the pulsar, with units of pc cm^{-3}. Its variation on year time scales is sensitive to fluctuations in plasma density on scales of $V_\perp/1$ yr, or $\sim 10^{14}$ cm for the pulsars in our sample. A typical line of sight, that toward pulsar 1937+21, shows variations of $\Delta DM \approx 6 \times 10^{-4}$ pc cm^{-3} (Rawley 1986), more than an order of magnitude less than those of the three pulsars in supernova remnants in Table 6.

Scattering by a supernova remnant around a pulsar may plausibly be described as a single thin screen at a distance, ζ from the pulsar. For $\zeta \ll D$, the expected temporal broadening is

$$\tau = \frac{\zeta}{2c} \psi_0 , \qquad (13)$$

where ψ_0 is the strength of scattering in the screen. Dispersion measure, in contrast, has a uniform weighting function along the line of sight. As a supernova remnant ages, we might expect τ to increase, as the screen moves further from the pulsar and ζ increases. If cosmic-ray acceleration in supernova remnants turns off when they reach a radius of ~ 50 pc, and if the observed enhanced scattering is a byproduct of this acceleration, one might expect τ to decline near that radius.

Temporal broadening increases approximately proportionately with age for the Crab and Vela pulsars; such behavior would be expected if the screen moves outward at constant speed and with constant strength of scattering ψ_1. The temporal broadening for pulsar 1951+32 falls well below the extrapolated value and is about that typical for sources at this distance (Cordes et al. 1985). This pulsar appears to have caught up with the expanding remnant; it appears in projection near its edge (Strom 1987). This geometry is expected to reduce ζ in equation (13) and so τ, below the value expected from the age and size of the remnant alone, but not by the factor of 100 observed relative to the Vela pulsar. The geometry should have no effect on ΔDM.

The data show significant differences among the scattering properties of the three remnants. They might indicate a trend of a steepening spectrum of density fluctuations with age, as α becomes more negative and fluctuations in dispersion measure become larger relative to temporal broadening. Age may not be the only independent variable. Our sample contains only three supernova remnants, and those three are quite different. The Crab supernova remnant is the archetypical pulsar-driven or "plerionic" remnant. The Vela SNR is more nearly a shell-type remnant, although it may have a plerionic component as well. CTB 80 may have been reenergized by its enclosed pulsar (Shull, Fesen, & Saken 1986); as noted above, geometry may reduce temporal broadening τ (although not ΔDM) for the 1951+32–CTB 80 pair.

5.3. *Radio-Wave Scattering by Supernova Remnants*

Lines of sight to pulsars or other compact radio sources that pass through supernova remnants by chance often show enhanced scattering, although clearcut associations of remnant and scattering, other than the two noted in this paper, are lacking. Dennison et al. (1984) noted a number of strongly scattered extragalactic sources seen through supernova remnants. Notably, the heavily scattered extragalactic source CL4 lies behind the Cygnus Loop supernova remnant (see also Fey, Spangler, & Mutel 1989). Spangler et al. (1986) observed strong scattering for two out of a sample of five extragalactic sources seen through or near supernova remnants. However, they also noted that the scattering might be due to incidental scattering along the lines of sight, rather than by the supernova remnants. Pulsar 1849+00 lies behind one of the remnants observed by Spangler et al., G33.6+0.1, and is heavily scattered (Frail & Clifton 1989). However, the nearby extragalactic source 1849+005 is also heavily scattered, although its line of sight does not pass through the remnant (Fey et al. 1991). Manchester, D'Amico, & Touhy (1985) found that the pulsar 1758−23,

behind the edge of supernova remnant W28, is heavily scattered.

6. CONCLUSIONS

We report angular broadening of eight pulsars by the interstellar plasma, measured with an intercontinental VLBI network at 326 MHz. Of these eight pulsars, four (1919+21, 1929+10, 2016+28, and 2020+28) are close to the speckle regime of interstellar scattering. In this regime, self-calibration of the complex gains of the antennas in the network, as we have done, removes the effects of scattering for a point source such as a pulsar. Thus, our observation that scattering disks of these pulsars are unresolved could be due either to an absence of angular broadening or to the effects of self-calibration. We find that four other pulsars (1642−03, 1818−04, 1933+16, and 1937+214) are moderately scattered and obtain measurements of their angular broadening. Measurements of the angular broadening of two pulsars (0531+21 and 0833−45) were previously reported in the literature. These two pulsars lie within associated supernova remnants, products of the explosions that produced the pulsars.

We discuss angular broadening of the pulsar and temporal broadening of the pulsar pulse. Both of these observables depend on the distribution of scattering material along the line of sight, but by different weighting functions. A third observable, the decorrelation bandwidth, is related to the temporal broadening by an uncertainty principle, and so has the same weighting function. We give expressions for the weighting functions in the general case and for the uniform-medium, thick-screen, and combined uniform-medium and thin-screen cases. Expressions for the thin-screen case are given by Desai et al. (1992).

We compare the measured angular broadening of the pulsars with temporal broadening as reported in the literature. We find that temporal and angular broadening of the four moderately scattered pulsars are consistent with a uniform distribution of scattering material using a weighting-function argument. Scattering of pulsar 1933+16 is mildly concentrated near the pulsar. Less significantly, the four pulsars close to the speckle regime are also consistent with a uniform distribution. The temporal broadening of 0531+21 can be divided into time-variable and time-constant parts; the angular broadening and the time-constant part of the temporal broadening of 0531+21 are ascribed to material distributed along the line of sight. The time-constant part of the scattering of 0531+21 is also consistent with a uniform distribution of scattering material. Results for the distributed component of scattering are consistent with a model for uniformly distributed scattering, with a localized scattering screen having ~ 3 times the strength of the uniform medium, $\psi_1/D\psi_0 = 3$. In the context of this model, applied to the five lines of sight, the strength of the screen lies between 1.9 and 3.7 times that of the extended medium, with 65% confidence. If effects of distance errors are taken into consideration, an analysis indicates the medium is probably even more uniform.

The supernova remnants associated with pulsars 0531+21 (Crab) and 0833−45 (Vela-X) scatter radiation from those pulsars strongly. This material is responsible for the time-variable part of scattering of 0531+21, and for most of the scattering of 0833−45. The proximity of the supernova remnants to pulsars reduces the effect of their strong scattering. If the scattering is modeled as a thin screen of strength ψ_1 and a uniform medium of strength $D\psi_0$, $\psi_1/D\psi_0 > 38$. The two supernova remnants have about the same strength of scattering. The material appears to be further away for the Vela pulsar, as expected from its greater age. The temporal broadening of the much older pulsar 1951+32, within the CTB 80 supernova remnant, is much less, only partly because the pulsar is near the edge of the remnant. The scattering and fluctuations in dispersion measure of these three pulsars due to their enclosing supernova remnants indicate a trend of relatively stronger large-scale ($l \sim 10^{14}$ cm) plasma fluctuations with increasing age.

Supernova remnants may accelerate cosmic rays by the first-order Fermi mechanism, in which particles are repeatedly reflected across a shock, thereby gaining energy from collisions with approaching matter on either side (Blandford & Eichler 1986). The accelerated particles should generate plasma fluctuations. These fluctuations may in turn reflect, and so ultimately accelerate, the particles (Bell 1978; Blandford & Ostriker 1978). This process is expected to operate most efficiently for supernova remnants 1–50 pc in size, or about the size of the Vela and Crab supernova remnants. Spangler et al. (1986) suggested that the plasma fluctuations might result in density fluctuations, which in turn would be observable through their effect on radio-wave propagation. The presence of strong scattering in or near these young supernova remnants suggests that we are indeed observing fluctuations accompanying acceleration of cosmic rays.

We thank G. Grove, R. Vernon, A. Wolszczan, and associates of the US VLBI Network for assistance with observations and correlation. We thank R. Blandford, R. Dewey, A. Fruchter, and J. Taylor for useful discussions, and the referee, S. R. Spangler, for an illuminating review. We thank C. Ryan for preparing many revisions of the manuscript. This research was supported in part by the National Science Foundation (AST 90-01426 and AST 92-17784).

REFERENCES

Alcock, C. R., & Hatchett, S. P. 1978, ApJ, 222, 456
Altunin, V. I. 1980, Soviet Astron., 25, 304
Alurkar, S. K., Slee, O. B., & Bobra, A. D. 1986, Australian J. Phys., 39, 133
Armstrong, J. W., & Coles, W. A. 1978, ApJ, 220, 346
Backer, D. C. 1974, ApJ, 190, 667
Backer, D. C., & Sramek, R. A. 1982, ApJ, 260, 512
Bell, A. R. 1978, MNRAS, 182, 147
Blandford, R. D., & Eichler, D. 1987, Phys. Rep., 154, 1
Blandford, R., & Narayan, R. 1985, MNRAS, 213, 591
Blandford, R. D., & Ostriker, J. P. 1978, ApJ, 221, L229
——. 1980, ApJ, 237, 793
Cohen, M. H., & Cronyn, W. M. 1974, ApJ, 192, 193
Cordes, J. M. 1986, ApJ, 311, 183
Cordes, J. M., Weisberg, J. M., & Boriakoff, V. 1985, ApJ, 288, 221
Cornwell, T. J., Anantharamaiah, K. R., & Narayan, R. 1989, JOSA, A 6, 977
Counselman, C. C., & Rankin, J. M. 1972, 166, 513
Dennison, B., Thomas, M., Booth, R. S., Brown, R. L., Broderick, J. J., & Condon, J. J. 1984, A&A, 135, 199
Desai, K. M., et al. 1992, ApJ, 393, L75
Fey, A. L., Spangler, S. R., & Cordes, J. M. 1991, ApJ, 372, 132
Fey, A. L., Spangler, S. R., & Mutel, R. L. 1989, ApJ, 337, 730
Foster, R. S., Backer, D. C., & Wolszczan, A. 1990, ApJ, 356, 243
Frail, D. A., & Clifton, T. R. 1989, ApJ, 336, 854
Frail, D. A., & Weisberg, J. M. 1990, AJ, 100, 743
Franson, C., & Epstein, R. I. 1980, ApJ, 242, 411
Fruchter, A. S., Taylor, J. H., Backer, D. C., Clifton, T. R., Foster, R. S., & Wolszczan, A. S. 1987, Nature, 331, 53
Graham, D. A., Mebold, U., Hesse, K. H., Hills, D. L., & Wielebinski, R. 1974, A&A, 37, 405
Gwinn, C. R., Cordes, J. M., Bartel, N., Wolszczan, A., & Mutel, R. L. 1988a, ApJ, 334, L13
Gwinn, C. R., Moran, J. M., & Reid, M. J. 1992, ApJ, 393, 149

Gwinn, C. R., Moran, J. M., Reid, M. J., & Schneps, M. H. 1988b, ApJ, 330, 817
Gwinn, C. R., Taylor, J. H., Weisberg, J. M., & Rawley, L. A. 1986, AJ, 91, 338
Hamilton, P. A., Hall, P. J., & Costa, M. E. 1985, MNRAS, 214, P5
Isaacman, R., & Rankin, J. M. 1977, ApJ, 214, 214
Kulkarni, S. R., Clifton, T. R., Backer, D. C., Foster, R. S., Frutcher, A. S., & Taylor, J. H. 1987, Nature, 330, 50
Lee, L. C., & Jokipii, J. R. 1976, ApJ, 206, 735
Lyne, A. G., Manchester, R. N., & Taylor, J. H. 1985, MNRAS, 213, 613
Lyne, A. G., Pritchard, R. S., & Smith, F. G. 1988, MNRAS, 233, 667
Lyne, A. G., & Smith F. G. 1990, Pulsar Astronomy (Cambridge Univ. Press)
Lyne, A. G., & Thorne, D. J., 1975, MNRAS, 172, 197
Manchester, R. N., D'Amico, N., & Tuohy, I. R. 1985, MNRAS, 212, 975
Montgomery, D., Brown, M. R., & Matthews, W. H. 1987, J. Geophys. Res., A92, 282
Mutel, R. L., Broderick, J. J., Carr, T. D., Lynch, M., Desch, M., Warnock, W. W., & Klemperer, W. K. 1974, ApJ, 193, 279
Mutel, R. L., & Lestrade, J.-F. 1990, ApJ, 349, L47
Narayan, R., & Goodman, J. 1989, MNRAS, 238, 963
Prentice, A. J. R., & ter Haar, D. 1969, MNRAS, 146, 423
Rao, A. P., Ananthakrishnan, S. 1984, Nature, 312, 707
Rawley, L. A. 1986, Ph.D. thesis, Princeton Univ.
Rawley, L. A., Taylor, J. H., & Davis, M. M. 1988, ApJ, 326, 947
Redhead, A. C. S., & Hewish, A. 1974, Nature, 236, 440
Reynolds, R. J. 1976, ApJ, 203, 151
Rickett, B. J. 1988, in The Impact of Very Long Baseline Interferometry on Astrophysics and Geophysics, ed. M. Reid & J. Moran (Dordrecht: Kluwer), 287
———. 1990, ARA&A, 28, 561
Rickett, B. J., Coles, W. A., & Bourgois, G. 1984, A&A, 134, 390
Salter, M. J., Lyne, A. G., & Anderson, B. 1979, Nature, 280, 477
Scheuer, P. A. G. 1968, Nature, 218, 920
Shull, J. M., Fesen, R. A., & Saken, J. M. 1986, ApJ, 346, 860
Spangler, S. R., Fey, A. L., & Cordes, J. M. 1987, ApJ, 322, 909
Spangler, S. R., & Gwinn, C. R. 1990, ApJ, 353, L29
Spangler, S. R., Mutel, R. L., Benson, J. M., & Cordes, J. M. 1986, ApJ, 301, 312
Strom, R. G. 1987, ApJ, 319, L103
Thompson, A. R., Moran, J. M., & Swenson, G. W., Jr. 1986, Interferometry and Synthesis in Radio Astronomy (New York: Wiley)
Vandenberg, N. R. 1976, ApJ, 209, 578
Vandenberg, N. R., Clark, T. A., Erickson, W. C., Resch, G. M., & Broderick, J. J. 1976, ApJ, 207, 937
Williamson, I. P. 1974, MNRAS, 166, 499